Wave-vortex interaction

Claudio Falcón[1,2] and Stéphan Fauve[1]

[1]*Laboratoire de Physique Statistique, École Normale Supérieure, CNRS, 24 rue Lhomond, 75 005 Paris, France*
[2]*Departamento de Física, Facultad de Ciencias Físicas y Matemáticas, Universidad de Chile, Casilla 487-3, Santiago, Chile*

We present an experimental study of the effect of an electromagnetically generated vortex flow on parametrically amplified waves at the surface of a vertically vibrated fluid layer. The underlying vortex flow, generated by a periodic Lorentz force, creates spatiotemporal fluctuations that nonlinearly interact with the standing surface waves. We measure the power spectral density of the surface wave amplitude and we characterize the bifurcation diagram by recording the subharmonic response of the surface to the external vibration. We show that the parametric instability is delayed in the presence of spatiotemporal fluctuations due to the vortex flow. In addition, the dependence of the amplitude of the subharmonic response on the distance to the instability threshold is modified. This shows that the nonlinear saturation mechanism of the waves is modified by the vortex flow.

I. INTRODUCTION

Waves on fluid interfaces are affected by the structure of the bulk flow [1]. Surface waves of wavelength λ and phase velocity c_λ can experience advection and eigenfrequency shifts due to the presence of a mean flow, thus changing the behavior and the properties of wave patterns. In the case of strongly fluctuating or even turbulent flows, the degree of complexity of wave propagation increases. Wave motion on the surface of a turbulent fluid has been a problem of interest since the early work of Phillips [2] on the scattering of a gravity surface wave of wavelength λ and phase velocity $c_\lambda = \sqrt{g\lambda/2\pi}$, by turbulent velocity fluctuations u_t in the limit $u_t \ll c_\lambda$. He pointed out the possibility of wave generation and wave dissipation induced by turbulent fluctuations, which has been experimentally studied later [3]. The aim of our work is to characterize the effect of turbulent fluctuations on a standing-wave pattern generated by a parametric instability. To that end we have studied parametrically amplified waves on a vertically vibrated fluid layer in the presence of an electromagnetically generated vortex flow.

It has been observed by Faraday that surface waves on a layer of fluid can be excited by periodically vibrating the fluid container [4]. When the vibration amplitude exceeds a critical value, he observed a standing-wave pattern oscillating at half the forcing frequency over the surface of the fluid. In the case of an inviscid fluid, it has been shown by Benjamin and Ursell that the amplitude of each normal mode of the free surface obeys a Mathieu equation; thus the instability mechanism is parametric amplification [5]. The effect of fluctuations on parametric instabilities has been studied theoretically [6] and experimentally [7–9]. In all these cases, the source of fluctuations has been either spatial or temporal. To our knowledge, the effect of externally imposed spatiotemporal fluctuations on a parametric instability has not been experimentally studied. Here, parametrically amplified surface waves are randomly forced by means of a periodic vortex flow. This fluctuating background flow is generated by a periodic Lorentz force acting on the fluid which supports the surface waves. In our experimental setup, the electromag-

netically induced velocity fluctuations of the vortex flow $\sigma(v)$ are small with respect to c_λ, as in [2]: the Froude number, $\mathrm{Fr} = \sigma(v)^2/c_\lambda^2$ is small ($\mathrm{Fr} \simeq 0.05$). The typical surface energy of the parametrically amplified waves is much larger than the kinetic energy of the fluctuating flow, as shown by the value of the Weber number, $\mathrm{We} = \rho\sigma(v)^2\lambda/\gamma \simeq 0.01$, where ρ is the fluid density and γ is its surface tension. Although we are in the limit of low We and Fr, the effect of the fluctuations of the vortex flow on the properties of parametrically amplified waves is not negligible.

In this paper, we show that the action of a fluctuating velocity field on parametrically amplified surface waves can inhibit the growth of the standing-wave pattern, thus increasing the instability threshold above its deterministic value. The manuscript is organized as follows. In Sec. II, we present the experimental setup and we describe the methods used to measure the velocity field v_1 generated by a periodic Lorentz force and the amplitude h_1 of the surface waves. In Sec. III, we study separately the effect of the parametric excitation and of the Lorentz force on the fluctuations of the free surface. The combined effect of both excitation mechanisms is studied in Sec. IV. We show that the parametric instability threshold increases when the underlying vortex flow is stronger. Finally, in Sec. V we present the conclusions and perspectives of this work.

II. EXPERIMENTAL SETUP AND MEASUREMENT TECHNIQUES

The experimental setup is displayed in Fig. 1. A Plexiglas container of 70×70 mm^2 is filled with mercury (density $\rho = 13.6 \times 10^3$ kg/m^3, kinematic viscosity $\nu = 1.2 \times 10^{-7}$ m^2/s, and surface tension $\gamma = 0.48$ N/m) up to a height $h_0 = 5$ mm. At the bottom of the cell, alternating vertical polarity magnets (diameter $\phi = 5$ mm, height $h = 8$ mm) made of neodymium and nickel coated are placed with a 1 mm gap between them in a hexagonal array (wavelength $\lambda = 6$ mm). The magnetic field strength at the surface of the fluid on top of a magnet is 500 G. Two nickel-barnished copper electrodes are glued at opposite sides of the
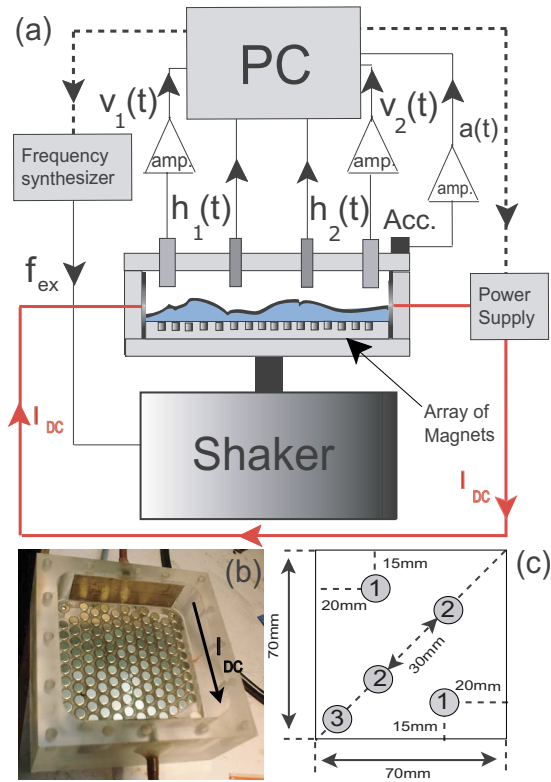
FIG. 1. (Color online) (a) Experimental setup. (b) Bottom of the experimental cell showing the hexagonal array of alternating polarity magnets, used to generate the periodic Lorentz force $\mathbf{F}_L$. The black arrow shows the sense of the applied dc current. (c) Top view of the cell showing the positions of the sensors: (1) Vivès probes, (2) inductive sensors, (3) accelerometer.

cell. A fine layer of Ni is deposited over them to prevent chemical reaction between mercury and copper. A dc current I of a few Amperes is applied through these electrodes, giving rise to a current density $\mathbf{j}$, and therefore a Lorentz force $\mathbf{F}_L = \mathbf{j} \times \mathbf{B}$, as shown in Fig. 1. The surface is kept clean by maintaining the fluid in a nitrogen-filled atmosphere and is temperature regulated by circulating water at 20.0 ± 0.1 °C. An electromagnetic vibration exciter, driven by a frequency synthesizer though a power amplifier, provides a clean vertical sinusoidal acceleration (horizontal acceleration less than 1% of the vertical one). The effective gravity in the reference frame of the container is then $g_{eff}(t) = g + a \cos(2\pi f_{ex}t)$, where g is the acceleration of gravity, a is proportional to the applied tension V with a 1.0 Vs^2/m sensitivity, and f_{ex} is the excitation frequency. The sinusoidal modulation of g is measured by a piezoelectric accelerometer and a charge amplifier. The surface wave amplitude is measured by two inductive sensors (eddy-current linear displacement gauge, Electro 4953 sensors with EMD1053 DC power supply). Both sensors, 3 mm in diameter, are screwed to the Plexiglas plate perpendicularly to the fluid surface at rest. They are put 0.7 mm above the surface on one diagonal of the cell, each one 15 mm away from its center (see Fig. 1). The linear sensing range of the sensors allows distance measurements from the sensor head to the fluid surface up to 1.27 mm with a 7.9 V/mm sensitivity. The linear response of these inductive sen-

sors in the case of a wavy liquid metal surface has been checked in a previous study [10].

In addition, local velocity fluctuations of the flow are measured by means of two Vivès probes [11]. They are placed on opposite sides of the container, 15 mm (respectively 20 mm) far from the closest walls and thus 50 mm far one from each other, as shown in Fig. 1. Each probe is made up by two copper wire electrodes plunging 2 mm into the fluid, separated by a distance $l = 3$ mm and isolated completely from the liquid metal, except at the very end, where the electrical contact is made. A small cylindrical magnet ($\phi = 5$ mm) is placed 5 mm above the electrodes, generating a magnetic field strength of 500 G at the electrical contact points. The whole system is integrated into a cylindrical rod that is screwed to the Plexiglas plate. For velocity fluctuations of length scales larger than l, the voltage difference measured between the electrodes is proportional to $v_1 B_0 l$, where v_1 is the velocity orthogonal to the vertical magnetic field B_0 generated by the probe's magnet [11,12]. For scales much smaller than l, the small-scale velocity fluctuations are spatially integrated by the probe. In frequency domain, this means that the transfer function of the probe is constant up to a cutoff frequency $f_c = \sigma(v_1)/2\pi l$, where $\sigma(v_1)$ is the *rms* value of the local velocity fluctuations. For frequencies larger than f_c, the transfer function of the probe decreases as f^{-2} [12]. For the data presented below, we have taken $v_1 = \Delta\Phi/lB_0$, where $\Delta\Phi$ is the voltage difference measured between the electrodes. The small voltage difference $\Delta\Phi$ of the order of a few microvolts is amplified by a factor of order 10^5 and acquired with the local height fluctuations and acceleration signals. The dc component of the signals is eliminated in the acquisition. The sampling frequency is fixed at 500 Hz in order to resolve the temporal fluctuations of the measured quantities and the acquisition time is 800 s, much larger than the typical time scales of the acquired signals.

III. EXPERIMENTAL RESULTS

We start by describing the flows generated when each forcing mechanism is applied alone. First, we describe the properties of the local wave amplitude of the parametrically amplified surface waves. Then, we consider the spatially periodic electromagnetic forcing alone.

A. Parametric excitation

The fluid container is vertically vibrated at frequency $f_{ex} = 23.8$ Hz and the amplitude a is increased. At a given threshold a_c, the flat surface becomes unstable to small perturbations and stationary surface waves appear, generating a pattern that oscillates at half the forcing frequency $f_{ex}/2 = 11.9$ Hz. In this experimental configuration, the geometry of the standing pattern is made of squares with a wavelength λ of order 7–8 mm without any defect. At this wavelength, gravity and capillarity are of comparable importance in the dispersion relation of the surface waves. The square pattern at onset is consistent with previous studies using mercury [13]. This results from the very low kinematic viscosity of mercury (one order of magnitude less than water). For fluids
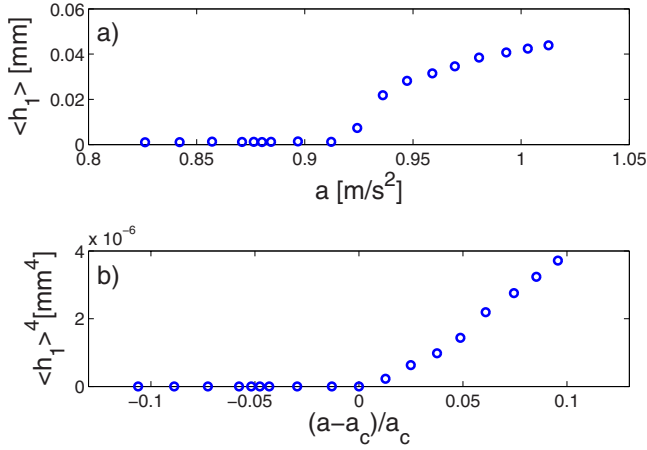
FIG. 2. (Color online) (a) Bifurcation diagram for the nonlinearly saturated wave amplitude $\langle h_1 \rangle$ as a function of a. (b) Bifurcation diagram for $\langle h_1 \rangle^4$ as a function of $\epsilon = (a - a_c)/a_c$.

with larger viscosities, patterns with different rotational orders have been observed and predicted [14]. The excitation frequency is chosen in order to have an eigenmode of standing surface waves over the container with a wavelength comparable to the one of the magnetic field **B**. In the explored frequency range ($20 < f_{ex} < 30$ Hz), the wavelength of parametrically amplified waves is roughly eight to ten times smaller that the size of the container. The frequency difference between two successive resonance tongues is about 1 Hz. By tuning the excitation frequency within a 1 Hz interval, it is easy to work in the vicinity of the minimum of a resonance tongue, i.e., without detuning between half the excitation frequency and the natural oscillation frequency of the surface waves. In this parameter range, the local amplitude of the surface waves $\langle h_1 \rangle$ does not present large scale modulations. We have used the Fourier amplitude of $h_1(t)$ at $f_{ex}/2$ by taking

$$\langle h_1 \rangle = \lim_{T \to \infty} \left| \frac{1}{2T} \int_{-T}^{T} h_1(t) e^{\pi i f_{ex} t} dt \right|,$$

where T is the acquisition time, much larger than the oscillation period π/f_{ex} ($T f_{ex} \sim 10^4$). The bifurcation diagram of the nonlinearly saturated wave amplitude is shown in Fig. 2. Its dependence on the reduced control parameter $\epsilon = (a - a_c)/a_c$ is proportional to $\epsilon^{1/4}$, as it has been previously reported [15]. This unusual scaling is observed because cubic nonlinearities vanish at zero detuning for parametric amplification in the limit of small dissipation. No distinguishable hysteresis loop is found in the measured bifurcation diagrams. Although the velocity signal related to the waves is rather small (mm/s), velocity measurements using the Vivès probes display the same bifurcation threshold for parametrically amplified waves as local amplitude recordings. The weakly nonlinear regime, with a nonlinearly saturated stationary standing wave, will be studied when fluctuations in space and time are added to the wave system, through an underlying vortex flow.

B. Vortex flow

We now study the fluctuations of the surface of the layer of mercury driven by a spatially periodic Lorentz force. When a current density **j** is applied through a liquid metal in the presence of a magnetic field **B**, a Lorentz force density $\mathbf{F}_L = \mathbf{j} \times \mathbf{B}$ sets the fluid in motion. In the present configuration, the current density **j** is generated by a constant dc current I applied through the mercury layer and its value is externally controlled by means of a power supply. As explained above, the magnetic field **B** is created by alternating polarity magnets arranged in a hexagonal lattice at the bottom of the container. Hence, $\mathbf{F}_L$ presents the same periodicity of **B** and generates a vortex flow which develops throughout the fluid perturbing the flat free surface and creating local height fluctuations. Small scale excitation using electromagnetic forcing has been used to study vortex dynamics [16,18] and quasi-two-dimensional turbulence [17]. The waves at the interface being of very small amplitude with respect to the depth of the mercury layer in our experimental setup, the current density **j** can be estimated as $\mathbf{j} = (I/S)\mathbf{e}$, where $S = 3.5 \times 10^{-4}$ m^2 is the surface crossed by the current and **e** is a unit vector pointing normally from one electrode (the cathode) to the other one (the anode). The velocity field **v** of the vortex flow can be estimated by balancing $\mathbf{F}_L$ and $\rho(\mathbf{v} \cdot \nabla)\mathbf{v}$ in the Navier-Stokes equation

$$\rho \left(\frac{\partial \mathbf{v}}{\partial t} + (\mathbf{v} \cdot \nabla)\mathbf{v} \right) = -\nabla p + \rho \nu \Delta \mathbf{v} + \mathbf{F}_L,$$

where ρ is the fluid density and ν is its kinematic viscosity. The order of magnitude for such velocity fluctuations at the forcing scale (the wavelength λ of the periodic magnetic field **B**) for a current I of order 1 A is 10^{-2} m/s, thus giving a Reynolds number Re of order 100. Even at low Re, the velocity field creates deformations on the free surface. Both surface and bulk fluctuations present large amplitude events and low-frequency fluctuations, as it is shown below.

1. Probability density functions

To study the statistical properties of the local response of the fluid to the periodic Lorentz force, we compute the probability density function (PDF) of both the local surface amplitude h_1 and the velocity field fluctuations v_1. We show their PDFs in Figs. 3 and 4 for different values of the dc current I. Increasing the value of I, larger and larger fluctuating events of local height and velocity occur. The rms value of local surface fluctuations $\sigma(h_1)$ increases with increasing current, as does the rms value of the local velocity fluctuations $\sigma(v_1)$. Their dependence on I is roughly linear (left inset in Figs. 3 and 4).

When plotted in the rescaled variables $h_1/\sigma(h_1)$ and $v_1/\sigma(v_1)$, all the PDFs collapse on one single curve (right inset in Figs. 3 and 4). No clear asymmetry is found in the normalized PDFs of both variables. A slight departure from the statistics of a random Gaussian variable is observed in both signals (the computed kurtosis is close to 3.2), but this is not large enough to discard gaussianity.
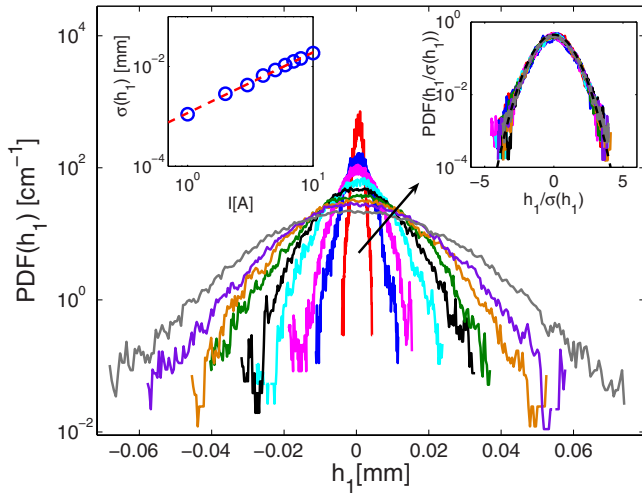
FIG. 3. (Color online) Probability density functions of the local amplitude fluctuations h_1 for different values of I between 1 and 9 A. The arrow shows the sense of increasing current. Left inset: Log-log plot of $\sigma(h_1)$ as a function of I. The best fit slope is 1.2. Right inset: Probability density functions of the rescaled local amplitude fluctuations $h_1/\sigma(h_1)$ for different values of I between 1 and 9 A. The dashed line represents a Gaussian fit.

2. Power spectral densities

As I is increased, low-frequency fluctuations dominate the response of the fluid motion to the Lorentz force $\mathbf{F}_L$. This is apparent in the power spectral densities (PSDs) of both h_1 and v_1 as shown in Fig. 5. When I is less than 1 A (not shown), there are peaks related to the lower normal modes of the surface waves in the container, excited by the fluctuations of the velocity field. At higher values of I ($I > 5$ A), this coherent response is completely lost. This shows that even at
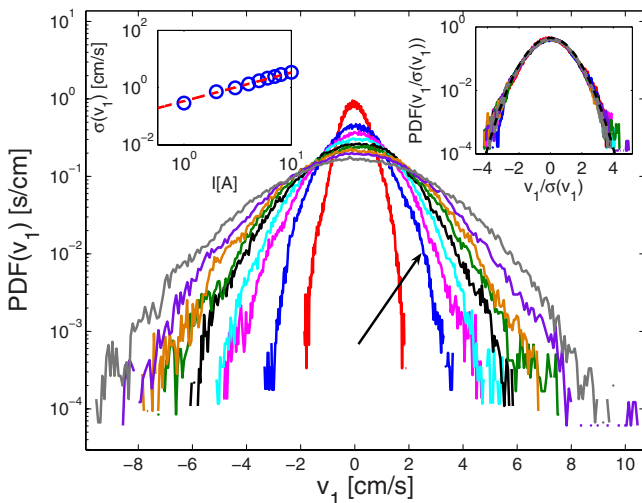

FIG. 4. (Color online) Probability density functions of the local velocity fluctuations v_1 for different values of I between 1 and 9 A. The arrow shows the sense of increasing current. Left inset: Log-log plot of the standard deviation $\sigma(v_1)$ as a function of I. The best fit slope is 1.0. Right inset: Probability density functions of the rescaled local velocity fluctuations $v_1/\sigma(v_1)$ for different values of I between 1 and 9 A. The dashed line represents a Gaussian fit.
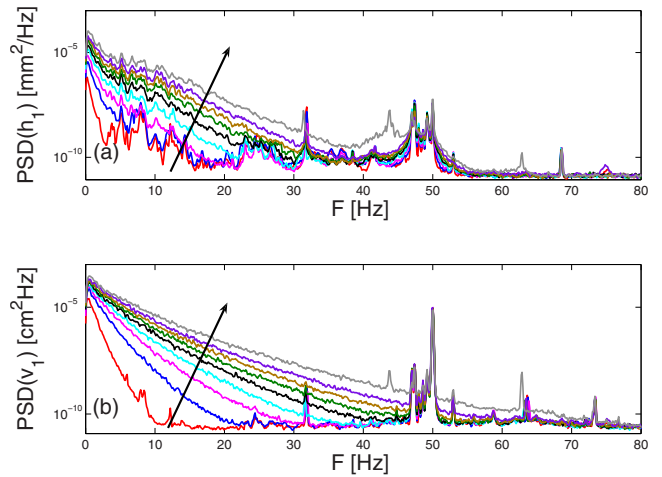

FIG. 5. (Color online) (a) Power spectral density the local wave amplitude fluctuations h_1 for different values of I between 1 and 9 A as a function of the frequency F. (b) Power spectral density the local velocity field fluctuations v_1 for different values of I between 1 and 9 A as a function of the frequency F. Arrows show the sense of increasing I.

moderate value of the Reynolds number (Re ~ 100), a chaotic behavior in time and space is achieved. We note that a qualitative difference between the spectra of surface deformation and velocity is visible despite their extension is less than half a decade. The spectra of h_1 display an exponential behavior and no power laws have been found even at large values of I (up to 20 A, not shown here). This is not the case for the spectra of v_1 that neither have an exponential nor a power-law behavior. Experiments with a larger setup will be performed to check whether this difference persists.

Rescaling the frequency by the typical turn-over time of the vortex flow, $\lambda/\sigma(v_1)$ (λ is the wavelength of the magnetic field) and the PSDs of the normalized variables $h_1/\sigma(h_1)$ and $v_1/\sigma(v_1)$ by their inverse frequency, we can try to collapse all the data on one single curve, as shown in Fig. 6. For the fluctuations of the local wave amplitude, there is a large dispersion for small values of I, due to the persistence of the cavity modes. As stated above, this coherent response is lost once the forcing is large enough ($I > 5$ A). On the other hand, all the velocity spectra collapse on one single curve.

IV. EFFECT OF SPATIOTEMPORAL FLUCTUATIONS INDUCED BY THE VORTEX FLOW ON PARAMETRIC SURFACE WAVES

Let us now study the effect of the velocity fluctuations driven by the periodic Lorentz force $\mathbf{F}_L$ on the growth, saturation, and statistics of parametrically forced surface waves. The wavelength of the standing pattern is chosen to be of the same order of magnitude as the one of the periodic vortex flow, forced at wavelength λ. This is done to maximize the effect of the vortex flow on the standing-wave pattern. In the presence of the spatiotemporal fluctuations generated by the vortex flow, the local amplitude h_1 of the surface waves strongly fluctuates as shown in Fig. 7. The PSD of h_1 is
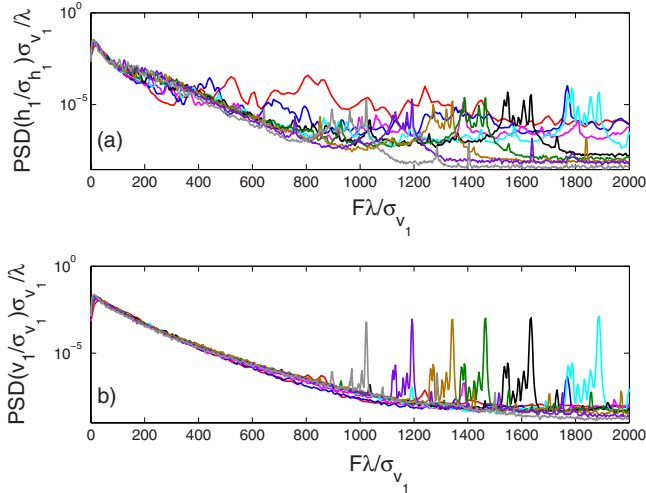
FIG. 6. (Color online) (a) Rescaled power spectral density of the normalized local wave amplitude fluctuations $h_1/\sigma(h_1)$ for different values of I between 1 and 10 A as a function of the normalized frequency $F\lambda/\sigma(v_1)$. (b) Rescaled power spectral density of the normalized local velocity field fluctuations $v_1/\sigma(v_1)$ for different values of I between 1 and 10 A as a function of the normalized frequency $F\lambda/\sigma(v_1)$.

displayed in Fig. 8 for increasing values of the current I that generates the vortex flow. We observe that the amplitude of the subharmonic response of the surface waves decreases when I is increased. Correspondingly, the width of the subharmonic response increases (see the inset of Fig. 8). On the other hand, the low-frequency part of the spectrum, which corresponds to the fluctuations generated by the Lorentz force, increases. For larger currents ($I > 2$ A), the amplitude of the subharmonic response disappears under the noise level of the fluctuations generated by the Lorentz force. The parametric amplification of surface waves is thus inhibited by the
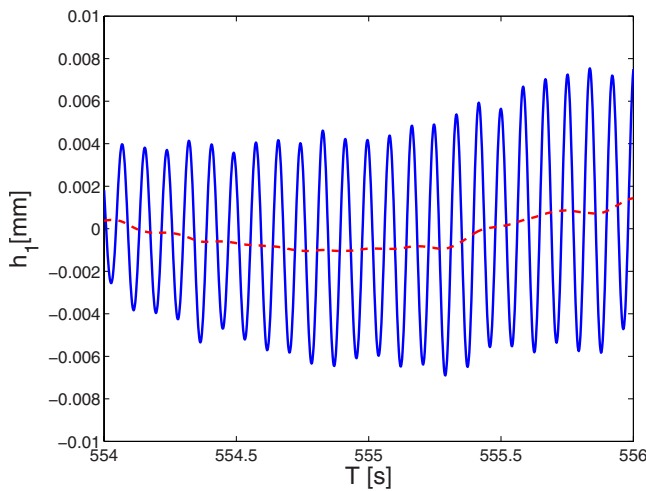

FIG. 7. (Color online) Direct recording of the local amplitude h_1 of the subharmonic response in presence of the vortex flow. The excitation frequency f_{ex} is 23.8 Hz and the dc current I is 1.0 A. Subharmonic oscillations (continuous line) are observed over superimposed low-frequency fluctuations (dashed line), which are computed by low-pass filtering h_1 at 5 Hz.
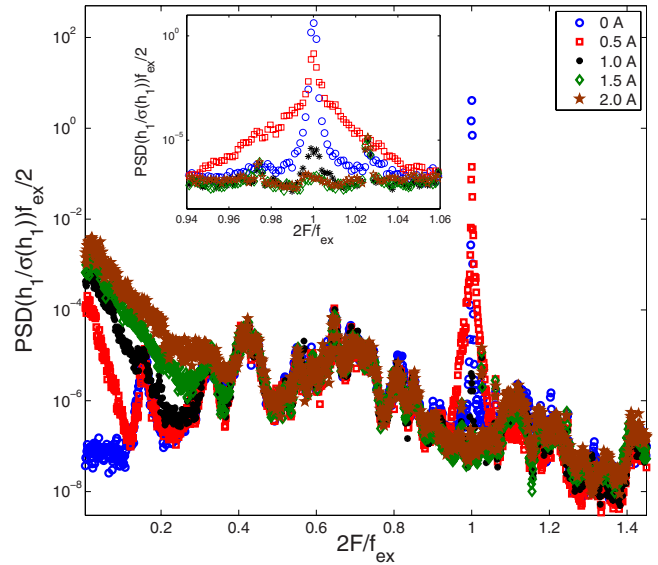

FIG. 8. (Color online) Power spectral density of the normalized local wave amplitude fluctuations $h_1/\sigma(h_1)$ for different values of the current intensity $I=0$ to 2 A as a function of the normalized frequency $2F/f_{ex}$ for a given value of $a > a_c$. Inset: Frequency window centered on the resonance peak of the parametric response for $I=0$ ($\bigcirc$), 0.5 ($\square$), 1.0 ($*$), 1.5 ($\diamondsuit$), and 2.0($\star$) A.

spatiotemporal fluctuations generated by the vortex flow.

In other words, the threshold of the parametric instability, i.e., the critical acceleration $a_c(I)$ for the onset of the subharmonic response, shifts to higher values with increasing values of I. This is shown by the bifurcation diagram displayed in Fig. 9, where we have plotted the Fourier coefficients at frequency $f_{ex}/2$ of the local wave amplitude, as described above. No distinguishable hysteresis loop is found. The sub-
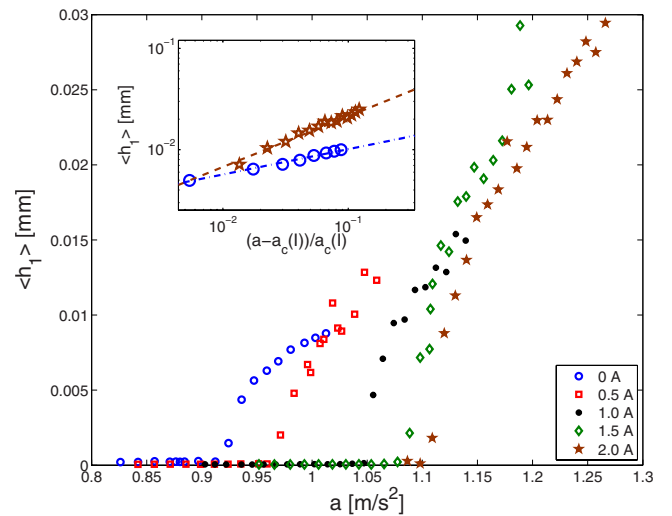

FIG. 9. (Color online) Bifurcation diagram of the subharmonic response $\langle h_1 \rangle$ of the local wave amplitude for $I=0$ ($\bigcirc$), 0.5 ($\square$), 1.0 ($*$), 1.5 ($\diamondsuit$), and 2.0($\star$) A. Inset: Log-log plot of the subharmonic response $\langle h_1 \rangle$ of the local wave amplitude as a function of the normalized acceleration $[a-a_c(I)]/a_c(I)$ for $I=0$ A ($\bigcirc$) and $I=2.0$ A ($\star$). Two power laws (dashed lines) are displayed with slopes 1/4 for $I=0$ A and 1/2 for $I=2.0$ A.
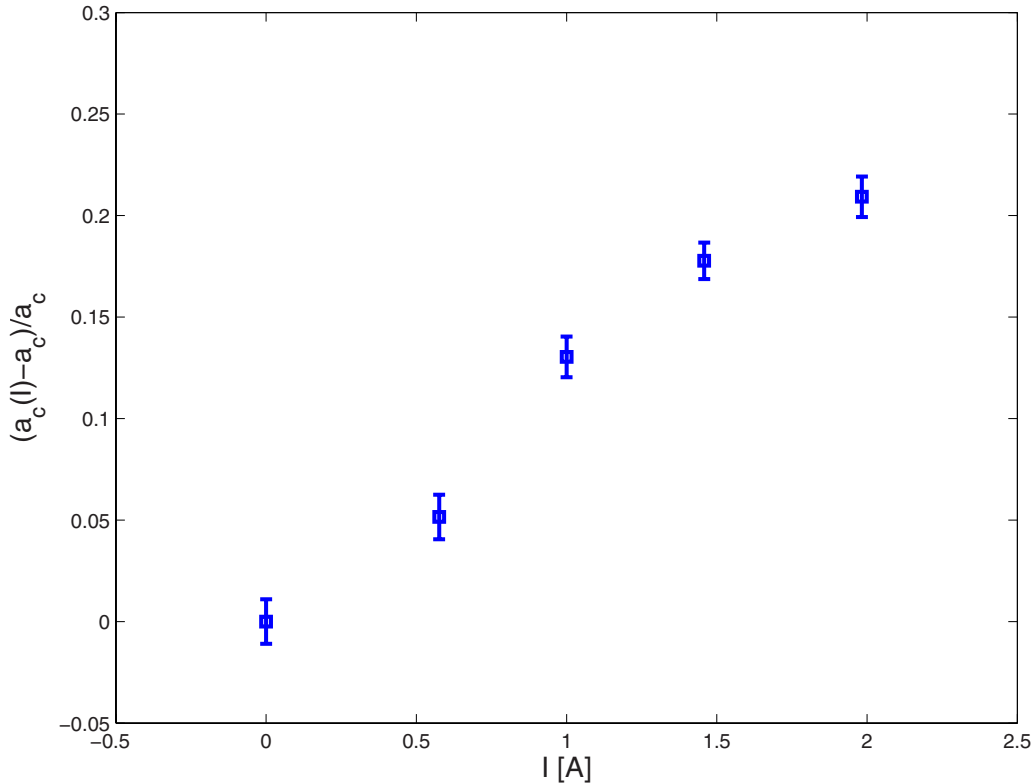
FIG. 10. (Color online) Normalized threshold growth $[a_c(I)-a_c]/a_c$ as a function of I ($\square$).

harmonic response $\langle h_1 \rangle$ is plotted as a function of the reduced control parameter $\epsilon(I)=[a-a_c(I)]/a_c(I)$ in the inset of Fig. 9. We observe that the dependence of $\langle h_1 \rangle$ on $\epsilon(I)$ changes when fluctuations related to the vortex flow increase: the 1/4 exponent for deterministic parametrically excited waves changes to 1/2 in the presence of the electromagnetic forcing. This is a strong indication of the modification of the saturation mechanism of parametrically amplified surface waves in the presence of spatiotemporal fluctuations generated by the vortex flow. From these bifurcation diagrams, we compute the threshold value $a_c(I)$ as a function of I in the range $0 < I < 2.0$ A. $a_c(I)$ is displayed in Fig. 10. We observe that the value of the parametric instability threshold is shifted by 20% for $I = 2$ A.

Two simple mechanisms can be considered in order to explain the shift in threshold and the modification of the exponent from 1/4 to 1/2 of the scaling of the parametric wave amplitude. First, random advection of the waves by the fluctuating vortices detunes the system away from parametric resonance. This leads to an increase of threshold. For instance, this type of mechanism explains the increase of threshold observed for parametric forcing in the presence of phase noise [15]. The modification of the exponent can be also ascribed to an effective detuning if it has the correct sign with respect to the nonlinear frequency correction. However, this has not been observed in the presence of phase noise. Another explanation for both the frequency shift and the modification of the exponent can be based on an increased effective viscosity of the waves related to the underlying flow. It is indeed known that the 1/4 exponent is observed at zero detuning only in the limit of small dissipation. It is likely that both mechanisms are involved, as for instance in the case where amplitude noise is added to parametric forcing. This indeed leads to both an effective detuning and dissipation [6].

V. CONCLUSIONS

We have studied two experimental configurations related to the problem of wave-vortex interaction. We have first shown how an electromagnetically driven array of vortices in a layer of mercury generates surface waves and we have studied their statistical properties. We have observed that they qualitatively differ from the ones of surface waves generated by vibrating paddles [19]. Although broad band spectra of the local wave amplitude are easily obtained as soon as the underlying flow is spatiotemporally chaotic, they display an exponential cutoff instead of a power-law decay observed for waves generated by vibrating paddles. The probability density functions of the local wave amplitude are also different: quasinormal PDFs, with a standard deviation linearly increasing with the driving current, are observed with electromagnetic forcing, whereas asymmetric PDFs have been reported in the case of vibrating paddles. We have also observed that the correlation length between the waves and the underlying flow is smaller than the size of the container in the presence of the fluctuating vortex flow. This has been also reported for waves generated by shear flows [20]. In our experiment, the forcing of the waves by the array of vortices inhibits freely propagating waves. Thus, a regime of weak turbulence is not observed.

Second, we have shown that the underlying vortex flow acts as a source of spatiotemporal fluctuations that inhibits parametrically amplified surface waves. It modulates the amplitude of the subharmonic response in a random way. The main effect of fluctuating vortices is to delay the threshold of the parametric instability. The vortex flow also affects the saturation mechanism of the local wave amplitude and qualitatively modifies the scaling of the amplitude of the parametric waves as a function of the reduced control parameter $\epsilon(I)$. In the presence of the vortex flow $\langle h_1 \rangle \sim \epsilon(I)^{1/2}$, whereas $\langle h_1 \rangle \sim \epsilon(I=0)^{1/4}$ for parametrically amplified surface waves without forcing by the vortices. This shows that the nonlinear saturation mechanism of the parametric waves qualitatively depends on the vortex flow.

[1] G. B. Whitham, *Linear and Nonlinear Waves*, 2nd ed. (Wiley, New York, 1999).

[2] O. M. Phillips, J. Fluid Mech. **5**, 177 (1959).

[3] A. Thackray, Nature (London) **237**, 115 (1972); S. V. Badulin, S. I. Voropaev, A. N. Kulikov, and A. D. Rozenberg, Oceanol. Acad. Sci. USSR **28**, 429 (1988); H. S. Olmez and J. H. Milgram, J. Fluid Mech. **239**, 133 (1992).

[4] M. Faraday, Philos. Trans. R. Soc. London **121**, 299 (1831).

[5] T. B. Benjamin and F. Ursell, Proc. R. Soc. London, Ser. A **225**, 505 (1954).

[6] R. L. Stratonovich, *Topics in the Theory of Random Noise* (Gordon and Breach, New York, 1963).

[7] S. Kabashima, S. Kogure, T. Kawakubo, and T. Okada, J. Appl. Phys. **50**, 6296 (1979); T. Kawakubo, A. Yanagita, and S. Kabashima, J. Phys. Soc. Jpn. **50**, 1451 (1981).

[8] V. V. Zautkin, B. I. Orel, and V. B. Cherepanov, Sov. Phys. JETP **58**, 414 (1983).

[9] S. Residori, R. Berthet, B. Roman, and S. Fauve, Phys. Rev. Lett. **88**, 024502 (2001); R. Berthet, A. Petrossian, S. Residori, B. Roman, and S. Fauve, Physica D **174**, 84 (2003).

[10] E. Falcon, C. Laroche, and S. Fauve, Phys. Rev. Lett. **89**, 204501 (2002).

[11] R. Ricou and C. Vivès, Int. J. Heat Mass Transfer **25**, 1579 (1982); A. Cramer, K. Varshney, T. Gundrum, and G. Gerbeth, Flow Meas. Instrum. **17**, 1 (2006).

[12] M. Berhanu, B. Gallet, N. Mordant and S. Fauve, Phys. Rev. E **78**, 015302(R) (2008).

[13] S. Ciliberto, S. Douady, and S. Fauve, Europhys. Lett. **15**, 23 (1991).

[14] A. Kudrolli and J. P. Gollub, Physica D **97**, 133 (1996); D. Binks and W. van de Water, Phys. Rev. Lett. **78**, 4043 (1997); P. Chen and J. Viñals, *ibid.* **79**, 2670 (1997).

[15] F. Petrélis, S. Aumaître, and S. Fauve, Phys. Rev. Lett. **94**, 070603 (2005).

[16] N. F. Bondarenko, M. Z. Gak, and F. V. Dolzhansky, Izv. Akad. Nauk (Fiz. Atmos. Okeana) **15**, 1017 (1979).

[17] J. Sommeria, J. Fluid Mech. **170**, 139 (1986).

[18] P. Tabeling, B. Perrin, and S. Fauve, Europhys. Lett. **3**, 459 (1987); O. Cardoso, H. Willaime, and P. Tabeling, Phys. Rev. Lett. **65**, 1869 (1990); P. Tabeling, O. Cardoso, and B. Perrin, J. Fluid Mech. **213**, 511 (1990).

[19] E. Falcon, C. Laroche, and S. Fauve, Phys. Rev. Lett. **98**, 094503 (2007); E. Falcon, S. Fauve, and C. Laroche, *ibid.* **98**, 154501 (2007).

[20] R. Savelsberg and W. van de Water, Phys. Rev. Lett. **100**, 034501 (2008).